Van Allen Probes Observations of a Three-Dimensional Field Line Resonance at a Plasmaspheric Plume

J. K. Sandhu[1], **A. W. Degeling[2]**, **T. Elsden[3]**, **K. R. Murphy[1,4,5]**, **I. J. Rae[1]**, **A. N. Wright[3]**, **D. P. Hartley[6]**, and **A. Smith[1]**

[1]Northumbria University, Newcastle upon Tyne, UK, [2]Institute of Space Science, Shandong University, Weihai, China, [3]School of Mathematics and Statistics, University of St Andrews, St Andrews, UK, [4]Self - Independent Researcher, Thunder Bay, ON, Canada, [5]Department of Physics, Lakehead University, Thunder Bay, ON, Canada, [6]Department of Physics and Astronomy, University of Iowa, Iowa City, IA, USA

Abstract Field Line Resonances (FLRs) are a critical component in Earth's magnetospheric dynamics, associated with the transfer of energy between Ultra Low Frequency waves and local plasma populations. In this study we investigate how the polarisation of FLRs are impacted by cold plasma density distributions during geomagnetic storms. We present an analysis of Van Allen Probe A observations, where the spacecraft traversed a storm time plasmaspheric plume. We show that the polarisation of the FLR is significantly altered at the sharp azimuthal density gradient of the plume boundary, where the polarisation is intermediate with significant poloidal and toroidal components. These signatures are consistent with magnetohydrodynamic modeling results, providing the first observational evidence of a 3D FLR associated with a plume in Earth's magnetosphere. These results demonstrate the importance of cold plasma in controlling wave dynamics in the magnetosphere, and have important implications for wave-particle interactions at a range of energies.

Plain Language Summary Earth's space environment is home to electrons and ions across a wide range of energies, trapped in the region by our global geomagnetic field. Energy can be transferred to and from the trapped particles through oscillations in the magnetic field, and these processes are responsible for the extreme energization of trapped electrons to hazardous levels for local spacecraft. In this paper we explore a type of magnetic field oscillation termed Field Line Resonances (FLRs): standing waves on a field line analogous to the oscillatory motion of guitar strings. We use spacecraft observations to show that the direction of the field line oscillations changes significantly depending on the density of the background plasma. The results confirm previous modeling work, and are the first observational evidence of 3D FLRs at a plume. The findings have important consequences for how FLRs transfer energy between the electrons and ions.

1. Introduction

The Earth's global geomagnetic field experiences an abundance of pulsations across a broad spectrum of frequencies. Electromagnetic pulsations with frequencies ranging from ~1–10 mHz are categorized as Ultra Low Frequency (ULF) waves (Jacobs et al., 1964). These ULF waves play a key role in a range of magnetospheric phenomena, such as radiation belt energization and transport (Brautigam & Albert, 2000; Ozeke & Mann, 2008; Sandhu, Rae, Wygant, et al., 2021; Turner et al., 2012), auroral substorms (Liang et al., 2009; Smith et al., 2020, 2023), and particle precipitation (Rae et al., 2018).

Uniquely to the ULF wave frequency band, the wavelengths are comparable to the scale size of the magnetospheric cavity, and Alfvén waves can form standing waves on closed geomagnetic field lines. These are termed Field Line Resonances (FLRs) (Dungey, 1954; Chen & Hasegawa, 1974; D. Southwood, 1974). FLRs have a direct relationship to the spatial distribution of cold plasma within the magnetosphere. The plasmasphere with a sharp, well-defined plasmapause can act as an inner cavity boundary for ULF waves and controls where FLRs can form (D. Southwood, 1974; Kivelson & Southwood, 1986; Rae et al., 2019; Wharton et al., 2020; Lee et al., 2002; Sandhu, Rae, Staples, et al., 2021). During geomagnetic storms, an enhanced convection electric field in the inner magnetosphere can dramatically distort the plasmasphere and result in the formation of a plasmaspheric plume in the afternoon sector (Chappell, 1972; Goldstein et al., 2019; Nishida, 1966; Sandhu et al., 2017). The plume is a region of high density plasma (~100 cm^{-3}) that typically extends from the plasmasphere to the dayside magnetopause.

Recent work indicates that the presence of a plasmaspheric plume has significant impacts on the propagation of ULF wave power through the inner magnetosphere (Degeling et al., 2018; Sandhu, Rae, Staples, et al., 2021). Elsden and Wright (2022) shows that the azimuthal asymmetries associated with the plume can have important consequences on the polarisation of a fast mode driven FLR across the plume boundary. Using a magnetohydrodynamic (MHD) simulation, Elsden and Wright (2022) observed that outside of a plume an FLR exhibited a predominantly toroidal polarisation (where the magnetic field perturbations were in the azimuthal direction). However, across the sharp density gradient at the plume boundary the FLR instead had an intermediate polarisation with perturbations both in the toroidal and poloidal (radial magnetic field perturbations) components. These FLRs are termed "3D FLRs," due to the equilibrium in which they exist depending on all three directions (Elsden et al., 2022; Wright & Elsden, 2016). Previous theory (e.g., Wright & Thompson, 1994) had only considered the "2D" problem, treating the plasma as invariant in the azimuthal direction and these 2D FLRs have an exclusively toroidal polarisation.

The FLRs considered by Elsden and Wright (2022) arise through the resonant coupling of externally driven fast mode waves to Alfvén waves. In contrast, high-m (where *m* refers to azimuthal wavenumber) poloidal FLRs are typically excited through resonant interactions with non-equilibrium particle distributions (D. J. Southwood & Hughes, 1983; Baddeley et al., 2005; James et al., 2016). Although the particle-driven waves are associated with different drivers and polarizations, they can also experience polarisation rotations similarly to the 3D FLRs proposed by Elsden and Wright (2022). In particular, analysis by Klimushkin et al. (1995) shows how the FLRs can rotate from a poloidal toward a toroidal polarisation (see also Leonovich & Mazur, 1993; Mager & Klimushkin, 2021). This phenomenon has also been demonstrated in simulations by Mann and Wright (1995) and observationally by Sarris et al. (2009) amongst many others, where the time-dependent phase mixing of a poloidal FLR is reported, although it is key that the polarisation change can be observed in an axisymmetric (2D) system. The 3D FLRs discussed in the remainder of this manuscript are distinct from these particle-driven waves. They are (a) FLRs driven by fast mode waves and (b) 3D FLRs generated through a non-axisymmetric density distribution (i.e., plasmaspheric plume). The externally driven waves play significant roles in magnetospheric dynamics during periods of enhanced solar wind coupling, and observationally have been assumed to be exclusively toroidal. The key idea of the new theory is that modes with a significant radial magnetic field component (azimuthal electric field) can be driven by the solar wind, allowing these azimuthal electric field components to accelerate/decelerate radiation belt electrons along their drift paths. We refer readers particularly to Elsden et al. (2022) for a relevant discussion of the differences between the particle-driven and fast mode driven FLRs.

The consequences of ULF wave polarisation variations are significant, where the polarisation is intimately linked to how ULF waves interact and resonate with local plasma (e.g., Degeling et al., 2008; Elkington et al., 2003). In this paper, we present the first observational evidence of a fast mode driven 3D FLR across a plume boundary, thus confirming the predictions of Elsden and Wright (2022) and asserting the importance of cold plasma in controlling the dynamics and polarisation of ULF waves.

2. Data and Methods

This study presents an analysis of observations between 16:10–19:25 on 26 August 2015. Magnetic field measurements are obtained by the Van Allen Probes A spacecraft (Mauk et al., 2013) using the Electric and Magnetic Field Instrument Suite and Integrated Science (EMFISIS) instrument (Kletzing et al., 2013, 2023). In order to determine the ULF wave field perturbations, the background field is taken as the running average over a 20 min sliding window (incremented by 1 min) and subtracted from the field measurements. The residual field is then transformed to a magnetic field-aligned coordinate system. The parallel component is defined to be aligned with the background field, the toroidal component is eastwards and perpendicular to the geocentric position vector, and the poloidal component completes the Cartesian system. For each component, the power spectral density in the ULF wave band (1–15 mHz) is also required. We use magnetic field power spectral density as derived by Murphy et al. (2023), which uses a Fourier Transform over a 20 min sliding (by 5 min) window. We note that azimuthal electric field observations of the ULF wave activity were not viable for this event, due to high errors in the spin axis electric field from the Electric Fields and Waves instrument (Wygant et al., 2013).

EMFISIS field observations are also used to infer concurrent measurements of the local total electron density. High frequency (10–500 kHz) electric field measurements are used to identify the upper hybrid resonance frequency, which is then used to infer the local electron density (Kurth et al., 2015). Traversals through different
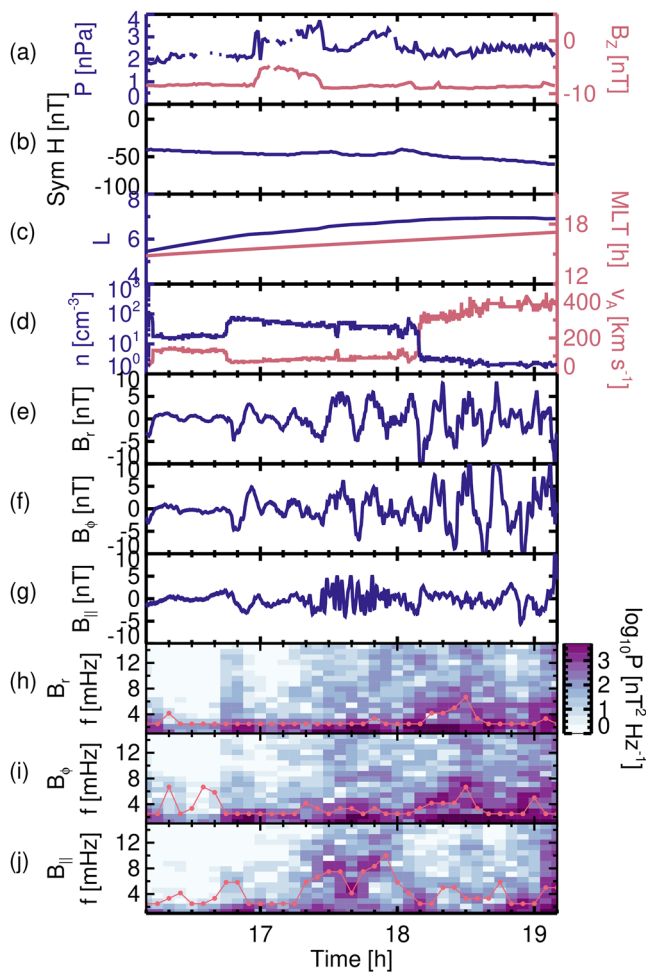
Figure 1. Observations between 16:10–19:10 on 26 August 2015. Timeseries are shown for (a) the solar wind dynamic pressure, P [nPa], (indigo) and the north-south interplanetary magnetic field component, B_Z, (pink); (b) the Sym H index [nT]; (c) the Van Allen Probes A L value (indigo) and magnetic local time (pink); (d) the electron density, n [cm^{-3}] (indigo) and the Alfvén speed, V_A [km s^{-1}] (pink); (e) the radial magnetic field component, B_r [nT]; (f) the azimuthal magnetic field component, B_ϕ [nT]; and (g) the compressional magnetic field component, $B_\parallel$ [nT]. Panels (h–j) show the power spectral density, P [nT^2 Hz^{-1}], for the radial, azimuthal, and compressional magnetic field components. The value of P is indicated by color, and the power is plotted as a function of time on the x-axis, with frequency, f [mHz], on the y axis. For each time step, the frequency at the maximum in P (for frequencies between 2 and 12 mHz) is marked by the pink profile.

plasma regimes, including crossings of the plasmapause and plasmaspheric plumes, are identified from timeseries of the electron density. For this event, the plume was identified from a plume crossing database (Hartley, 2022).

3. Results

We present evidence of a 3D FLR situated on the edge of a plasmaspheric plume, as observed by the Van Allen Probes A spacecraft. Figure 1 shows observations between 16:10–19:10 on 26 August 2015, where Figure 1a shows the solar wind dynamic pressure, P [nPa], (indigo) and the interplanetary magnetic field (IMF) north-south component, B_Z [nT] (pink) as observed by the ACE spacecraft. At ∼16:55, an impulsive peak in the solar wind dynamic pressure is observed where the pressure increases from approximately 2 to 4 nPa. This enhancement in P is accompanied by a decrease in the magnitude of southward B_Z from 8.5 to 5 nT. Following the solar wind structure, the conditions remain relatively steady for the remainder of the interval.

Figure 1b shows the Sym H index (Iyemori, 1990) remained steady at approximately −50 nT throughout the event. The Sym H variation over a wider time period (not shown) indicates the observations are taken during the main phase of a geomagnetic storm where the Sym H index reached a minimum value of −101 nT.

Figure 1c displays the location of the spacecraft in L (indigo) and Magnetic Local Time (MLT, pink) coordinates. The probe was passing into apogee with L increasing from approximately 5 to 7, with MLT increasing from 15 to 18, and firmly in the afternoon sector where plumes are most commonly observed (Darrouzet et al., 2008; K.-C. Kim & Shprits, 2019; Hartley et al., 2022). Figure 1d shows the local electron density, n [cm^{-3}] (indigo). The probe crosses from the plasmasphere to the low density plasmatrough at 14:25 (not shown), allowing us to be confident that the subsequent density gradients are not plasmapause boundary crossings. At 16:45, the probe crosses into a plasmaspheric plume with the density increasing from 20 to 80 cm^{-3}. The probe moves duskwards, exits the plume at 18:10 with the density reducing to 2 cm^{-3}, and the probe remains in the plasmatrough for the remainder of the event. We also show the estimated Alfvén speed, v_A [km s^{-1}] (pink), calculated from the local magnetic field strength and electron density from EMFISIS and the ion composition from the Helium, Oxygen, Proton, and Electron (HOPE) ion spectrometer onboard the Van Allen Probes (Funsten et al., 2013). The density (and hence Alfvén speed) gradients associated with the plume crossings are sharp, and the gradient is particularly significant for the duskward crossing (18:10). Due to the elevated convection electric field associated with the strongly negative IMF B_Z, the plume is dynamic and has significantly thinned and diffused in the following hours when the plume is next sampled by Van Allen Probe B (not shown here) (Borovsky & Denton, 2008; Goldstein & Sandel, 2005).

Figures 1e and 1f shows the radial, B_r [nT], azimuthal, B_ϕ [nT], and compressional, $B_\parallel$ [nT] magnetic field components, and Figures 1h–1j shows the corresponding power spectral density, P [nT^2 Hz^{-1}], for each component as a function of time and frequency, f [mHz]. The frequency bin corresponding to the maximum power at each timestep is marked (pink profile, Figures 1h–1j) to guide the eye to features in the spectrograms. Enhancements in wave activity across all components are observed following the solar wind impulse, including a patch of elevated compressional wave power at ∼17:40, denoting that the ULF waves are driven externally (K.-H. Kim et al., 2002; Oliveira et al., 2020). A lack of any "bump-on-tail" features in particle data (not shown) provide further evidence that the perturbations arise from solar wind driving. Clear continuous waveforms are apparent in the radial and azimuthal components (Figures 1e and 1f). Enhanced wave power at $f \sim 6$ mHz can be identified from the radial
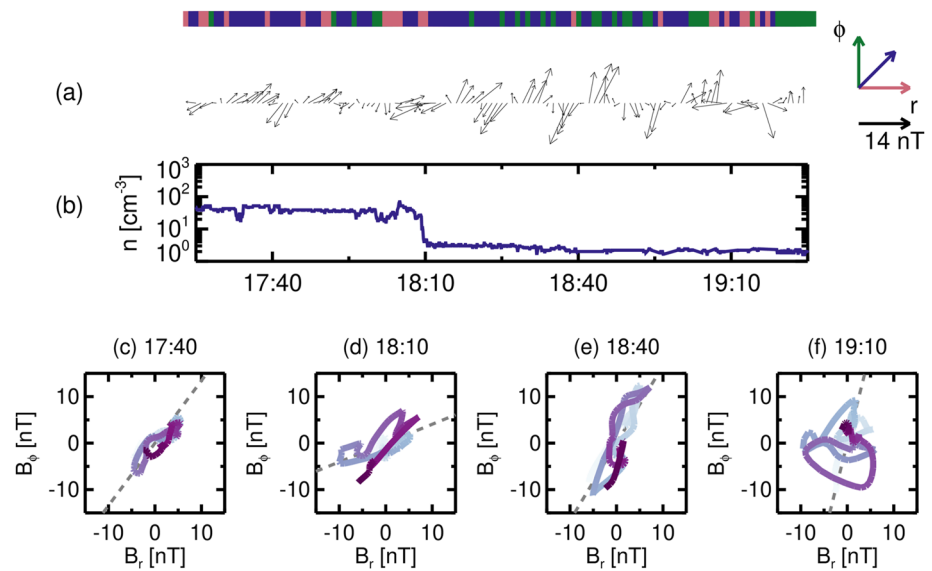
Figure 2. Magnetic field and electron density observations between 17:25–19:25 on 26 August 2015. Panel (a) shows the magnetic field vectors in the radial (*x*-direction) and azimuthal (*y*-direction) as a function of time, using a 5 min sampling interval. The magnitude of the vectors correspond to the scale shown on the right of the panel. Color coding above the panel describes the angle of the vector measured from the *y*-axis. Green for $0 \pm 22.5°$; indigo for $45 \pm 22.5°$; and pink for $90 \pm 22.5°$. Panel (b) shows the electron density, n [cm^{-3}], as a function of time. Panels (c–f) show hodograms, where the radial and azimuthal field components, B_r and B_ϕ [nT], respectively, are plotted for a 30 min interval. The midpoint time of the interval is labeled at the top of each panel. The color of the trace indicates the time from the start (light blue) to the end (dark purple) of the interval. The dashed lines in each panel show the major axis.

and azimuthal components at roughly 18:10 (Figures 1h and 1i) when the probe exits the plume, suggesting the presence of a FLR at and around the plume boundary. A comparison of the radial and azimuthal components also show that the fluctuations are roughly in phase. The quadrature in time of the magnetic field with the electric field provides further evidence of a standing wave structure (see Supporting Information S1 for details).

Although there is notable ULF wave activity and evidence of FLRs observed during the duskward plume crossing at ∼18:10, there are limited features of interest seen in the noonside crossing at ∼16:45. This is attributed to the noonside crossing occurring prior to the solar wind impulse, such that the ULF wave activity is comparatively minimal. As such, we will focus only on the duskward plume crossing in the analysis that follows.

3.1. A Change in FLR Polarisation

Figure 2 shows how the polarisation of the FLR changes as the probe crosses the duskside plume boundary at 18:10, showing observations from 17:25 to 19:25. Figure 2a shows the magnetic field vector as a function of time, using a cadence of 5 min. The x-component corresponds to the radial direction and the y-component corresponds to the azimuthal direction. The color coding at the top of the panel provides a rough guide on the polarisation. Time stamps are colored according to polarisation, with pink and green representing dominant radial and azimuthal components, respectively. If the angle between the field vector and the *x*-axis is within 22.5° of 45°, then the radial and azimuthal components are comparable and the timestamp is colored indigo. The polarisation can then be described as intermediate and the FLR is a 3D FLR. Figure 2b shows the electron density, n [cm^{-3}], for context. We can see that very close to and at the crossing (18:10), the polarisation is intermediate and the timestamps are colored indigo. At earlier times, the vector magnitudes are reduced and there are no obviously consistent features in the polarisation. At later times (18:20–19:00), the polarisation is much more azimuthally aligned, also indicated by the recurrent green patches in the colored time stamps. From 19:00, the polarisation is unclear and the vectors dramatically shrink in magnitude.

We suggest that the external source of fast mode ULF wave power propagated from the dayside magnetosphere, accumulated around the plasmapause boundary (Degeling et al., 2018), and then coupled to drive FLRs in the vicinity of the boundary. Strong amplitude fluctuations in the transverse magnetic field are observed in this

region (∼18:10–19:00). Deep within the plume comparatively minimal field oscillations and low wave power are observed, which may be due to the sharp density gradients at the plume boundaries acting to reflect/redirect any externally propagating compressional ULF waves and prevent access to the high density plume region (Degeling et al., 2018; Lee et al., 2002).

To further understand changes in the polarisation we include hodogram analysis in Figures 2c–2f. The time period from 17:25 to 19:25 is subdivided into 4 intervals of 30 min duration (capturing multiple wave periods), where each interval corresponds to a different panel. The magnetic field is plotted as a function of the radial and azimuthal components, and higher frequency oscillations (≥8 mHz) are removed to focus on ULF wave frequencies where high wave power is seen (Figures 1h and 1i). The resulting ellipses illustrate key features. Narrow ellipses are present when the radial and azimuthal oscillations are in phase or anti-phase, whereas broad ellipses indicate the components are in lagging/leading quadrature. The orientation/tilt of the ellipses represent the polarisation, showing which component(s) that the field perturbations occur in. To describe the polarisation, the major axis is shown by the dashed lines in each hodogram. The major axis is defined here as the angle that the largest magnitude field vector in the 30 min interval makes with the y-axis. A line with this angle is extrapolated, giving the dashed lines in each panel. Although Figures 2c–2f show that the polarisation is sometimes unclear or variable throughout the interval, the major axis is useful for roughly quantifying the polarisation when appropriate.

Figure 2c shows that well within the plume the amplitude of the field perturbations is small, as previously discussed. The polarisation angle is ∼37°, indicating the field oscillations occur in both components. At the plume boundary, the polarisation angle is increased to 68°, where Figure 2d shows the perturbation has both strong radial and azimuthal components that is characteristic of a 3D FLR. The intermediate polarisation is seen throughout the 30 min interval, indicating that the width of the 3D FLR region is broad compared to the density gradient (also evident in Figure 2a). Beyond the plume boundary and firmly in the low density plasmatrough, the polarisation angle is markedly reduced to 31° and the field perturbations are strongly dominant in the azimuthal direction (Figure 2e). Figure 2f shows that moving even further away from the plume region, and further in time from the solar wind impulse, that the perturbations are no longer linear and there is no clear polarisation of FLRs. Figure 1j also shows that the compressional magnetic field component fluctuations increase in amplitude from approximately 18:50, such that fast mode waves may be distorting and broadening the hodogram shown in Figure 2f (Elsden & Wright, 2022).

The approximately linear polarisation (i.e., narrow ellipses) and orientation of the hodograms in Figure 2c indicate that the radial and azimuthal field components are roughly in phase in the 3D FLR region. This is also apparent from the timeseries shown in Figures 1e and 1f, and confirms the modeling predictions of Elsden and Wright (2022) (see Figures 3 and 6 of Elsden and Wright (2022)). In brief, the Elsden and Wright (2022) model results show that on the dusk-side plume edge the contour of a fixed Alfvén frequency is orientated in the positive radial and positive azimuthal direction due to the negative density gradient in the azimuthal direction. Therefore, the transverse field and velocity components will be directed positively in both the radial and azimuthal directions when crossing the plume, and hence will be in phase. In contrast, the different Alfvén frequency contour for a dawn-side plume crossing indicates the radial and azimuthal field components would be out of phase in that case.

3.2. Variations in FLR Frequency

A key component of FLR theory is that a given field line can support a standing Alfvén wave at a frequency that depends on the polarisation angle. Therefore, the field line can host FLRs at a range of frequencies corresponding to a minimum and maximum polarisation angle. The analysis of Elsden and Wright (2022) showed that field lines at an azimuthal density gradient (and hence Alfvén speed gradient) can adopt an intermediate polarisation, such that it can support an FLR at the driving frequency.

To establish how the observed FLRs vary in frequency-space, we estimate the range of possible frequencies of the traversed field lines using a model for shear Alfvén wave (SAW) eigenmodes in an arbitrary background magnetic field by combining the approaches of Wright et al. (2022) and Degeling et al. (2018). This model assumes infinite conductivity ionospheres, and requires the background magnetic field (and field line geometry) and plasma density profile along field lines in the vicinity of the satellite location to be specified. The former is given by the T96 magnetic field model (Tsyganenko, 1995; Tsyganenko & Stern, 1996), and the latter is assumed to have a power-law scaling with geocentric radius along the magnetic field, which is normalized by the observed density
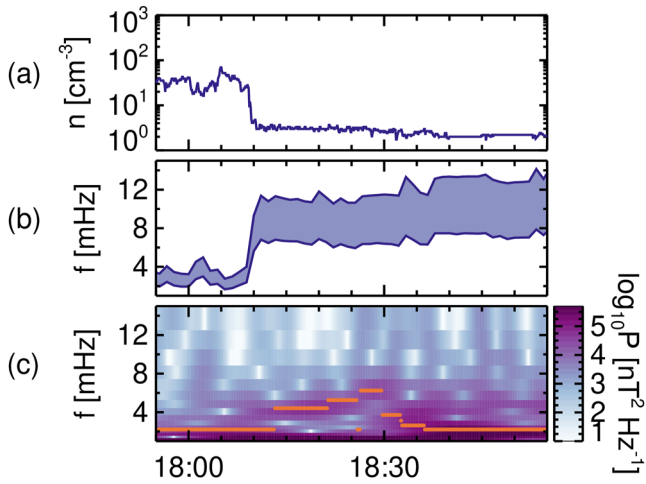
Figure 3. Data and model timeseries between 17:55 and 18:55 on 26 August 2015. Panel (a) shows electron density, n [cm^{-3}]. Panel (b) shows the range of polarisation dependent modeled frequencies on the spacecraft's field line, and panel (c) shows the power spectral density P [nT^2 Hz^{-1}] of the transverse magnetic field component. For each time step, the frequency at the maximum in P is marked in pink (for frequencies between 2 and 12 mHz).

value at the satellite location. The maximum and minimum Alfvén frequencies are found by solving the eigenvalue equation resulting from Equation 3 in Degeling et al. (2018), by setting the external driver current and fast mode parallel magnetic field component equal to zero, then finding the two lowest frequency eigenmodes. These correspond to half-wavelength solutions with "poloidal-like" and "toroidal-like" polarizations, and their frequencies agree with the maximum and minimum Alfvén frequencies, as found in Wright et al. (2022) (see Elsden et al. (2022)).

Figure 3 shows the results, where the electron density, n [cm^{-3}], is shown in Figure 3a for context. Figure 3b shows the estimated model frequency range, f [mHz], of the field lines for this interval, as indicated by the shaded region. The frequency range extends from the most poloidal FLR (minimum frequency) to the most toroidal FLR (maximum frequency) for the spacecraft's position. This shaded region can be considered a resonant band, showing where the field lines can resonate at in spectral space. Figure 3c shows the observed power spectral density, P [nT^2 Hz^{-1}], for the transverse component (both the radial and azimuthal components) of the observed magnetic field. The power spectral density was determined using a wavelet transform and is plotted as a function of frequency, f [mHz], and time. The time interval shown in Figure 3 corresponds to the period encompassed by Figures 2d and 2e where the polarization change is observed.

The modeling results show that the resonant band experiences significant variations during the plume boundary crossing. Inside the plume (before 18:10), the frequencies range from approximately 3 to 4 mHz. Outside the plume (after 18:10) the density drops by an order of magnitude, forcing a jump in the band such that it spans frequencies from approximately 6 to 12 mHz.

The corresponding observational frequency dependences are shown in Figure 3c. We note a band of high power at low frequencies (∼2 mHz) throughout the interval, which is below the expected fundamental mode FLR frequency for this event, and is posited to potentially be quarter mode resonances located close to the dusk terminator (e.g., Obana et al., 2008). Therefore, the low frequency region has been excluded in this analysis to focus on the higher harmonic FLR fluctuations. The FLR frequency manifests in Figure 3c as a high power band that increases in frequency with time, apparent from ∼18:00 to 18:30 (see pink profile). The FLR frequency increases from approximately 3 mHz at the plume boundary to approximately 8 mHz outside of the plume. We note that, qualitatively, the observations in Figure 3c agree with the model outputs (Figure 3b), such that the FLR frequency increases in the low density plasmatrough compared to the high density plume. However, it is also noted that the observed frequencies are lower than the model estimates outside of the plume, where the quasi-toroidal wave frequency should be toward the upper bound of the band and close to 12 mHz. We suggest the model-observations difference may arise from model inputs (e.g., oversimplified ion composition description). Overall, we show that the observations exhibit both the expected change in polarisation and frequency when traversing the density gradient as a 3D FLR, with similarities and differences to the modeled estimates.

4. Conclusions

We present observations of a clear and broad 3D FLR at the edge of a plasmaspheric plume, supported by a sharp density gradient. This event study directly confirms predictions made by Elsden and Wright (2022), and is the first observational evidence of a 3D FLR associated with a plume. This 3D FLR has a polarisation that is between the extremes of purely toroidal and poloidal, and is driven by a fast mode wave (rather than driven by particle interactions).

As well as further emphasizing the capabilities of MHD simulations to predict and characterize key properties of magnetospheric ULF waves (e.g., Archer et al., 2022; Claudepierre et al., 2016; Degeling et al., 2018; Wright & Elsden, 2020), these results highlight key open questions in inner magnetospheric science.

1. *What are the implications of 3D FLRs on the local plasma*? Both toroidal and poloidal mode FLRs can resonantly interact with local plasma populations across a range of energies. Drift or drift-bounce resonances are implicated in

radiation belt transport and energization (Elkington et al., 2003), acceleration of plasmaspheric ions and electrons (Ren et al., 2017; Zong et al., 2012), and drift-bounce resonance with ring current plasma (James et al., 2016; Yang et al., 2010; Yeoman & Wright, 2001). However, these interactions are sensitively dependent on the polarisation and frequency of the FLRs (Elkington et al., 2003). The presence of 3D FLRs alters the resonance contours and the resonant energies of the local plasma population (Elsden & Wright, 2022; Wright et al., 2022). Understanding the implications of these changes in a realistic storm time environment is a fundamental question, that will have consequences for multiple inner magnetospheric phenomenon (e.g., radiation belt energization and ring current decay).

However, the single event study presented here raises the question of how common these 3D FLRs are? Although it is outside the scope of this report to perform a detailed statistical analysis of when and where 3D FLRs occur during storms (which will form future studies), it is expected that the occurrence of 3D FLRs is highly dependent on the presence of solar wind driven fast mode waves to couple to the FLR but also without distorting the hodogram signatures (Elsden & Wright, 2022). Veritably, initial surveys confirm that whilst 3D FLRs occur under certain conditions, they are not present for all plume crossings. Future studies will also benefit from concurrent simulation work to fully understand how plume properties (e.g., density gradients and plume locations) will affect the likelihood of 3D FLRs forming and being observable.

2. *How do plumes impact other wave processes*? These results illustrate one aspect of how plumes can have significant ramifications for the propagation and coupling of ULF waves. This highlights the importance of continued active research into understanding how other wave modes can also be affected by cold density structures. For example, Hartley et al. (2022) observed changes in the obliquity of chorus waves close to plume boundaries with implications for the chorus-to-hiss mechanism (Hartley et al., 2019). Fully understanding how plumes alter the behavior of the range of wave processes in the inner magnetosphere (e.g., ULF waves, chorus waves, hiss waves, ion cyclotron waves, magnetosonic waves) will significantly reshape our knowledge of radiation belt dynamics, where variations in the radiation belt result from multiple different wave processes acting in tandem (Baker, 2021). Furthermore, including plumes in models of wave diffusion coefficients that are used in radiation belt modeling, will allow us to evaluate the role they play in wider radiation belt dynamics and improve modeling capabilities.

3. *Improved characterization of the storm-time cold plasma density distribution*. Although plumes are a relatively common feature during geomagnetic storms (Li et al., 2022) and play a significant role in a range of inner magnetospheric phenomena, they are often omitted from cold plasma distribution models (e.g., Gallagher et al., 2000; Hartley et al., 2023; Sandhu et al., 2017; Sheeley et al., 2001). Current advances include work by Goldstein et al. (2014), where test particle simulations reproduce the shape of the plasmapause and plume boundaries to within 0.4 R_E, although descriptions of densities within the plumes, plasmasphere, and plasmatrough are not included yet. Empirical modeling using neural networks shows promising progress in this area (James et al., 2021; Zhelavskaya et al., 2017, 2021). The SPICED model by James et al. (2021) and the PINE model by Zhelavskaya et al. (2017) are able to describe density distributions for the plasmasphere and plasmatrough as well as detailing the broad shape of the plume during storms. Future work to extend these models, quantify accuracy during disturbed periods, and focus on fully capturing the storm time plume structure would be highly beneficial. Accurate density models that realistically describe plume shape, size, and density gradients would allow step-change advancements in the empirical diffusion coefficients used in radiation belt modeling, by including these unique wave-particle interactions in and around plasmaspheric plumes. A key route for improved density modeling is improved cold plasma measurements. Propositions for in situ and imaging observations of cold plasma in the inner magnetosphere, such as the PILOT mission concept (Malaspina et al., 2022), would be invaluable in better understanding the dynamics of cold plasma, as well as supporting existing data sets (e.g., Van Allen Probes and Arase (Miyoshi et al., 2017)) in investigating impacts of cold plasma on wave processes.

To conclude, we have presented the first direct observations of a 3D FLR at a plume. The observations demonstrate that plumes play a critical role in the propagation and coupling of ULF waves in the inner magnetosphere. The results reaffirm the importance of accurately characterizing storm time cold plasma distribution for more realistic empirical models, as well as highlighting questions around the impacts of 3D FLRs on our current understanding of ULF waves and their interactions with local plasma populations.

Data Availability Statement

Van Allen Probes and Sym H data is available from Coordinated Data Analysis Web (CDAWeb) [Dataset] (2023). The solar wind data is publicly available from NASA/GSFC's Space Physics Data Facility's OMNIWeb service (Papitashvili & King, 2020). The Van Allen Probes plume crossing list is provided by Hartley (2022).

References

Archer, M. O., Southwood, D. J., Hartinger, M. D., Rastaetter, L., & Wright, A. N. (2022). How a realistic magnetosphere alters the polarizations of surface, fast magnetosonic, and Alfvén waves. *Journal of Geophysical Research: Space Physics*, *127*(2), e2021JA030032. https://doi.org/10.1029/2021JA030032

Baddeley, L. J., Yeoman, T. K., & Wright, D. M. (2005). Hf Doppler sounder measurements of the ionospheric signatures of small scale ULF waves. *Annales Geophysicae*, *23*(5), 1807–1820. https://doi.org/10.5194/angeo-23-1807-2005

Baker, D. N. (2021). Wave–particle interaction effects in the van Allen belts. *Earth Planets and Space*, *73*(1), 189. https://doi.org/10.1186/s40623-021-01508-y

Borovsky, J. E., & Denton, M. H. (2008). A statistical look at plasmaspheric drainage plumes. *Journal of Geophysical Research*, *113*(A9), A09221. https://doi.org/10.1029/2007JA012994

Brautigam, D. H., & Albert, J. M. (2000). Radial diffusion analysis of outer radiation belt electrons during the October 9, 1990, magnetic storm. *Journal of Geophysical Research*, *105*(A1), 291–309. https://doi.org/10.1029/1999JA900344

CDAWEB. (2023). Coordinated data analysis web (CDAWEB) [Dataset]. GSFC. Retrieved from https://cdaweb.gsfc.nasa.gov

Chappell, C. R. (1972). Recent satellite measurements of the morphology and dynamics of the plasmasphere. *Reviews of Geophysics*, *10*(4), 951–979. https://doi.org/10.1029/RG010i004p00951

Chen, L., & Hasegawa, A. (1974). A theory of long-period magnetic pulsations: 1. Steady state excitation of field line resonance. *Journal of Geophysical Research*, *79*(7), 1024–1032. https://doi.org/10.1029/JA079i007p01024

Claudepierre, S. G., Toffoletto, F. R., & Wiltberger, M. (2016). Global MHD modeling of resonant ULF waves: Simulations with and without a plasmasphere. *Journal of Geophysical Research: Space Physics*, *121*(1), 227–244. https://doi.org/10.1002/2015JA022048

Darrouzet, F., De Keyser, J., Décréau, P. M. E., El Lemdani-Mazouz, F., & Vallières, X. (2008). Statistical analysis of plasmaspheric plumes with cluster/whisper observations. *Annales Geophysicae*, *26*(8), 2403–2417. https://doi.org/10.5194/angeo-26-2403-2008

Degeling, A. W., Ozeke, L. G., Rankin, R., Mann, I. R., & Kabin, K. (2008). Drift resonant generation of peaked relativistic electron distributions by Pc 5 ULF waves. *Journal of Geophysical Research*, *113*(A2), A02208. https://doi.org/10.1029/2007JA012411

Degeling, A. W., Rae, I. J., Watt, C. E. J., Shi, Q. Q., Rankin, R., & Zong, Q.-G. (2018). Control of ULF wave accessibility to the inner magnetosphere by the convection of plasma density. *Journal of Geophysical Research: Space Physics*, *123*(2), 1086–1099. https://doi.org/10.1002/2017JA024874

Dungey, J. W. (1954). Electrodynamics of the outer atmosphere. In *Pennsylvania state university ionosphere research laboratory science report* (Vol. 69).

Elkington, S. R., Hudson, M. K., & Chan, A. A. (2003). Resonant acceleration and diffusion of outer zone electrons in an asymmetric geomagnetic field. *Journal of Geophysical Research*, *108*(A3), 1116. https://doi.org/10.1029/2001JA009202

Elsden, T., Wright, A., & Degeling, A. (2022). A review of the theory of 3-D Alfvén (field line) resonances. *Frontiers in Astronomy and Space Sciences*, *9*. https://doi.org/10.3389/fspas.2022.917817

Elsden, T., & Wright, A. N. (2022). Polarization properties of 3-d field line resonances. *Journal of Geophysical Research: Space Physics*, *127*(2), e2021JA030080. https://doi.org/10.1029/2021JA030080

Funsten, H. O., Skoug, R. M., Guthrie, A. A., MacDonald, E. A., Baldonado, J. R., Harper, R. W., et al. (2013). Helium, oxygen, proton, and electron (hope) mass spectrometer for the radiation belt storm probes mission. *Space Science Reviews*, *179*(1), 423–484. https://doi.org/10.1007/s11214-013-9968-7

Gallagher, D. L., Craven, P. D., & Comfort, R. H. (2000). Global core plasma model. *Journal of Geophysical Research*, *105*(A8), 18819–18833. https://doi.org/10.1029/1999JA000241

Goldstein, J., Pascuale, S., & Kurth, W. S. (2019). Epoch-based model for stormtime plasmapause location. *Journal of Geophysical Research: Space Physics*, *124*(6), 4462–4491. https://doi.org/10.1029/2018JA025996

Goldstein, J., Pascuale, S. D., Kletzing, C., Kurth, W., Genestreti, K. J., Skoug, R. M., et al. (2014). Simulation of van Allen probes plasmapause encounters. *Journal of Geophysical Research: Space Physics*, *119*(9), 7464–7484. https://doi.org/10.1002/2014JA020252

Goldstein, J., & Sandel, B. R. (2005). The global pattern of evolution of plasmaspheric drainage plumes. In *Inner magnetosphere interactions: New perspectives from imaging* (pp. 1–22). American Geophysical Union (AGU). https://doi.org/10.1029/159GM02

Hartley, D. P. (2022). List of plasmaspheric plumes from van Allen probes (RBSP) [Dataset]. University of Iowa. https://doi.org/10.25820/data.006173

Hartley, D. P., Chen, L., Christopher, I. W., Kletzing, C. A., Santolik, O., Li, W., & Shi, R. (2022). The angular distribution of lower band chorus waves near plasmaspheric plumes. *Geophysical Research Letters*, *49*(9), e2022GL098710. https://doi.org/10.1029/2022GL098710

Hartley, D. P., Cunningham, G. S., Ripoll, J.-F., Malaspina, D. M., Kasahara, Y., Miyoshi, Y., et al. (2023). Using van Allen probes and Arase observations to develop an empirical plasma density model in the inner zone. *Journal of Geophysical Research: Space Physics*, *128*(3), e2022JA031012. https://doi.org/10.1029/2022JA031012

Hartley, D. P., Kletzing, C. A., Chen, L., Horne, R. B., & Santolík, O. (2019). Van Allen probes observations of chorus wave vector orientations: Implications for the chorus-to-hiss mechanism. *Geophysical Research Letters*, *46*(5), 2337–2346. https://doi.org/10.1029/2019GL082111

Iyemori, T. (1990). Storm-time magnetospheric currents inferred from mid-latitude geomagnetic field variations. *Journal of Geomagnetism and Geoelectricity*, *42*(11), 1249–1265. https://doi.org/10.5636/jgg.42.1249

Jacobs, J. A., Kato, Y., Matsushita, S., & Troitskaya, V. A. (1964). Classification of geomagnetic micropulsations. *Journal of Geophysical Research*, *69*(1), 180–181. https://doi.org/10.1029/JZ069i001p00180

James, M. K., Yeoman, T. K., Jones, P., Sandhu, J. K., & Goldstein, J. (2021). The scalable plasma ion composition and electron density (spiced) model for earth's inner magnetosphere. *Journal of Geophysical Research: Space Physics*, *126*(9), e2021JA029565. https://doi.org/10.1029/2021JA029565

James, M. K., Yeoman, T. K., Mager, P. N., & Klimushkin, D. Y. (2016). Multiradar observations of substorm-driven ULF waves. *Journal of Geophysical Research: Space Physics*, *121*(6), 5213–5232. https://doi.org/10.1002/2015JA022102

Kim, K.-C., & Shprits, Y. (2019). Statistical analysis of hiss waves in plasmaspheric plumes using van allen probe observations. *Journal of Geophysical Research: Space Physics*, *124*(3), 1904–1915. https://doi.org/10.1029/2018JA026458

Kim, K.-H., Cattell, C. A., Lee, D.-H., Takahashi, K., Yumoto, K., Shiokawa, K., et al. (2002). Magnetospheric responses to sudden and quasiperiodic solar wind variations. *Journal of Geophysical Research*, *107*(A11), SMP36–1–SMP36-12. https://doi.org/10.1029/2002JA009342

Kivelson, M. G., & Southwood, D. J. (1986). Coupling of global magnetospheric MHD eigenmodes to field line resonances. *Journal of Geophysical Research*, *91*(A4), 4345–4351. https://doi.org/10.1029/JA091iA04p04345

Kletzing, C. A., Bortnik, J., Hospodarsky, G., Kurth, W. S., Santolik, O., Smitth, C. W., et al. (2023). The electric and magnetic fields instrument suite and integrated science (EMFISIS): Science, data, and usage best practices. *Space Science Reviews*, *219*(4), 28. https://doi.org/10.1007/s11214-023-00973-z

Kletzing, C. A., Kurth, W. S., Acuna, M., MacDowall, R. J., Torbert, R. B., Averkamp, T., et al. (2013). The electric and magnetic field instrument suite and integrated science (EMFISIS) on RBSP. *Space Science Reviews*, *179*(1), 127–181. https://doi.org/10.1007/s11214-013-9993-6

Klimushkin, D. Y., Leonovich, A. S., & Mazur, V. A. (1995). On the propagation of transversally small-scale standing Alfvén waves in a three-dimensionally inhomogeneous magnetosphere. *Journal of Geophysical Research*, *100*(A6), 9527–9534. https://doi.org/10.1029/94JA03233

Kurth, W. S., De Pascuale, S., Faden, J. B., Kletzing, C. A., Hospodarsky, G. B., Thaller, S., & Wygant, J. R. (2015). Electron densities inferred from plasma wave spectra obtained by the waves instrument on van Allen probes. *Journal of Geophysical Research: Space Physics*, *120*(2), 904–914. https://doi.org/10.1002/2014JA020857

Lee, D.-H., Hudson, M. K., Kim, K., Lysak, R. L., & Song, Y. (2002). Compressional MHD wave transport in the magnetosphere 1. Reflection and transmission across the plasmapause. *Journal of Geophysical Research*, *107*(A10), SMP16-1–SMP16-14. https://doi.org/10.1029/2002JA009239

Leonovich, A., & Mazur, V. (1993). A theory of transverse small-scale standing alfvén waves in an axially symmetric magnetosphere. *Planetary and Space Science*, *41*(9), 697–717. https://doi.org/10.1016/0032-0633(93)90055-7

Li, H., Fu, T., Tang, R., Yuan, Z., Yang, Z., Ouyang, Z., & Deng, X. (2022). Statistical study and corresponding evolution of plasmaspheric plumes under different levels of geomagnetic storms. *Annales Geophysicae*, *40*(2), 167–177. https://doi.org/10.5194/angeo-40-167-2022

Liang, J., Liu, W. W., Donovan, E. F., & Spanswick, E. (2009). In-situ observation of ULF wave activities associated with substorm expansion phase onset and current disruption. *Annales Geophysicae*, *27*(5), 2191–2204. https://doi.org/10.5194/angeo-27-2191-2009

Mager, P. N., & Klimushkin, D. Y. (2021). The field line resonance in the three-dimensionally inhomogeneous magnetosphere: Principal features. *Journal of Geophysical Research: Space Physics*, *126*(1), e2020JA028455. https://doi.org/10.1029/2020JA028455

Malaspina, D., Ergun, R., Goldstein, J., Spittler, C., Andersson, L., Borovsky, J., et al. (2022). Plasma imaging, local measurement, and tomographic experiment (pilot): A mission concept for transformational multi-scale observations of mass and energy flow dynamics in earth's magnetosphere. *Frontiers in Astronomy and Space Sciences*, *9*. https://doi.org/10.3389/fspas.2022.910730

Mann, I. R., & Wright, A. N. (1995). Finite lifetimes of ideal poloidal alfvén waves. *Journal of Geophysical Research*, *100*(A12), 23677–23686. https://doi.org/10.1029/95JA02689

Mauk, B. H., Fox, N. J., Kanekal, S. G., Kessel, R. L., Sibeck, D. G., & Ukhorskiy, A. (2013). Science objectives and rationale for the radiation belt storm probes mission. *Space Science Reviews*, *179*(1), 3–27. https://doi.org/10.1007/s11214-012-9908-y

Miyoshi, Y., Kasaba, Y., Shinohara, I., Takashima, T., Asamura, K., Matsumoto, H., et al. (2017). Geospace exploration project: Arase (ERG). *Journal of Physics: Conference Series*, *869*(1), 012095. https://doi.org/10.1088/1742-6596/869/1/012095

Murphy, K. R., Sandhu, J. K., Rae, I. J., Daggitt, T. A., Glauert, S. A., Horne, R. B., et al. (2023). A new four-component l*-dependent model for radial diffusion based on solar wind and magnetospheric drivers of ULF waves. *ESS Open Archive*. https://doi.org/10.22541/essoar.167591092.27672309/v1

Nishida, A. (1966). Formation of plasmapause, or magnetospheric plasma knee, by the combined action of magnetospheric convection and plasma escape from the tail. *Journal of Geophysical Research*, *71*(23), 5669–5679. https://doi.org/10.1029/JZ071i023p05669

Obana, Y., Menk, F. W., Sciffer, M. D., & Waters, C. L. (2008). Quarter-wave modes of standing Alfvén waves detected by cross-phase analysis. *Journal of Geophysical Research*, *113*(A8), A08203. https://doi.org/10.1029/2007JA012917

Oliveira, D. M., Hartinger, M. D., Xu, Z., Zesta, E., Pilipenko, V. A., Giles, B. L., & Silveira, M. V. D. (2020). Interplanetary shock impact angles control magnetospheric ULF wave activity: Wave amplitude, frequency, and power spectra. *Geophysical Research Letters*, *47*(24), e2020GL090857. https://doi.org/10.1029/2020GL090857

Ozeke, L. G., & Mann, I. R. (2008). Energization of radiation belt electrons by ring current ion driven ULF waves. *Journal of Geophysical Research*, *113*(A2), A02201. https://doi.org/10.1029/2007JA012468

Papitashvili, N. E., & King, J. H. (2020). Omni 1-min data set [Dataset]. NASA Space Physics Data Facility. https://doi.org/10.48322/45bb-8792

Rae, I. J., Murphy, K. R., Watt, C. E., Sandhu, J. K., Georgiou, M., Degeling, A. W., et al. (2019). How do ultra-low frequency waves access the inner magnetosphere during geomagnetic storms? *Geophysical Research Letters*, *46*(19), 10699–10709. https://doi.org/10.1029/2019GL082395

Rae, I. J., Murphy, K. R., Watt, C. E. J., Halford, A. J., Mann, I. R., Ozeke, L. G., et al. (2018). The role of localized compressional ultra-low frequency waves in energetic electron precipitation. *Journal of Geophysical Research: Space Physics*, *123*(3), 1900–1914. https://doi.org/10.1002/2017JA024674

Ren, J., Zong, Q.-G., Miyoshi, Y., Zhou, X. Z., Wang, Y. F., Rankin, R., et al. (2017). Low-energy (<200 eV) electron acceleration by ULF waves in the plasmaspheric boundary layer: Van Allen probes observation. *Journal of Geophysical Research: Space Physics*, *122*(10), 9969–9982. https://doi.org/10.1002/2017JA024316

Sandhu, J. K., Rae, I. J., Staples, F. A., Hartley, D. P., Walach, M.-T., Elsden, T., & Murphy, K. R. (2021). The roles of the magnetopause and plasmapause in storm-time ULF wave power enhancements. *Journal of Geophysical Research: Space Physics*, *126*(7), e2021JA029337. https://doi.org/10.1029/2021JA029337

Sandhu, J. K., Rae, I. J., Wygant, J. R., Breneman, A. W., Tian, S., Watt, C. E. J., et al. (2021). Ulf wave driven radial diffusion during geomagnetic storms: A statistical analysis of van Allen probes observations. *Journal of Geophysical Research: Space Physics*, *126*(4), e2020JA029024. https://doi.org/10.1029/2020JA029024

Sandhu, J. K., Yeoman, T. K., Rae, I. J., Fear, R. C., & Dandouras, I. (2017). The dependence of magnetospheric plasma mass loading on geomagnetic activity using cluster. *Journal of Geophysical Research: Space Physics*, *122*(9), 9371–9395. https://doi.org/10.1002/2017JA024171

Sarris, T. E., Wright, A. N., & Li, X. (2009). Observations and analysis of Alfvén wave phase mixing in the earth's magnetosphere. *Journal of Geophysical Research*, *114*(A3), A03218. https://doi.org/10.1029/2008JA013606

Sheeley, B. W., Moldwin, M. B., Rassoul, H. K., & Anderson, R. R. (2001). An empirical plasmasphere and trough density model: CRRES observations. *Journal of Geophysical Research*, *106*(A11), 25631–25641. https://doi.org/10.1029/2000JA000286

Smith, A. W., Rae, I. J., Forsyth, C., Watt, C. E. J., & Murphy, K. R. (2020). On the magnetospheric ULF wave counterpart of substorm onset. *Journal of Geophysical Research: Space Physics*, *125*(4), e2019JA027573. https://doi.org/10.1029/2019JA027573

Smith, A. W., Rae, I. J., Forsyth, C., Watt, C. E. J., & Murphy, K. R. (2023). Statistical characterization of the dynamic near-earth plasma sheet relative to ultra-low frequency (ULF) wave growth at substorm onset. *Journal of Geophysical Research: Space Physics*, *128*(1), e2022JA030491. https://doi.org/10.1029/2022JA030491

Southwood, D. (1974). Some features of field line resonances in the magnetosphere. *Planetary and Space Science*, *22*(3), 483–491. https://doi.org/10.1016/0032-0633(74)90078-6

Southwood, D. J., & Hughes, W. J. (1983). Theory of hydromagnetic waves in the magnetosphere. *Space Science Reviews*, *35*(4), 301–366. https://doi.org/10.1007/BF00169231

Tsyganenko, N. A. (1995). Modeling the earth's magnetospheric magnetic field confined within a realistic magnetopause. *Journal of Geophysical Research*, *100*(A4), 5599–5612. https://doi.org/10.1029/94JA03193

Tsyganenko, N. A., & Stern, D. P. (1996). Modeling the global magnetic field of the large-scale birkeland current systems. *Journal of Geophysical Research*, *101*(A12), 27187–27198. https://doi.org/10.1029/96JA02735

Turner, D. L., Shprits, Y., Hartinger, M., & Angelopoulos, V. (2012). Explaining sudden losses of outer radiation belt electrons during geomagnetic storms. *Nature Physics*, *8*(3), 208–212. https://doi.org/10.1038/nphys2185

Wharton, S. J., Rae, I. J., Sandhu, J. K., Walach, M.-T., Wright, D. M., & Yeoman, T. K. (2020). The changing eigenfrequency continuum during geomagnetic storms: Implications for plasma mass dynamics and ULF wave couping. *Journal of Geophysical Research: Space Physics*, *125*(6), e2019JA027648. https://doi.org/10.1029/2019JA027648

Wright, A., Degeling, A. W., & Elsden, T. (2022). Resonance maps for 3D Alfvén waves in a compressed dipole field. *Journal of Geophysical Research: Space Physics*, *127*(4), e2022JA030294. https://doi.org/10.1029/2022JA030294

Wright, A. N., & Elsden, T. (2016). The theoretical foundation of 3D Alfvén resonances: Normal modes. *Astrophysical Journal*, *833*(2), 230. https://doi.org/10.3847/1538-4357/833/2/230

Wright, A. N., & Elsden, T. (2020). Simulations of MHD wave propagation and coupling in a 3-D magnetosphere. *Journal of Geophysical Research: Space Physics*, *125*(2), e2019JA027589. https://doi.org/10.1029/2019JA027589

Wright, A. N., & Thompson, M. J. (1994). Analytical treatment of Alfvén resonances and singularities in nonuniform magnetoplasmas. *Physics of Plasmas*, *1*(3), 691–705. https://doi.org/10.1063/1.870815

Wygant, J. R., Bonnell, J. W., Goetz, K., Ergun, R. E., Mozer, F. S., Bale, S. D., et al. (2013). The electric field and waves instruments on the radiation belt storm probes mission. *Space Science Reviews*, *179*(1), 183–220. https://doi.org/10.1007/s11214-013-0013-7

Yang, B., Zong, Q.-G., Wang, Y. F., Fu, S. Y., Song, P., Fu, H. S., et al. (2010). Cluster observations of simultaneous resonant interactions of ULF waves with energetic electrons and thermal ion species in the inner magnetosphere. *Journal of Geophysical Research*, *115*(A2), A02214. https://doi.org/10.1029/2009JA014542

Yeoman, T. K., & Wright, D. M. (2001). Ulf waves with drift resonance and drift-bounce resonance energy sources as observed in artificially-induced HF radar backscatter. *Annales Geophysicae*, *19*(2), 159–170. https://doi.org/10.5194/angeo-19-159-2001

Zhelavskaya, I. S., Aseev, N. A., & Shprits, Y. Y. (2021). A combined neural network- and physics-based approach for modeling plasmasphere dynamics. *Journal of Geophysical Research: Space Physics*, *126*(3), e2020JA028077. https://doi.org/10.1029/2020JA028077

Zhelavskaya, I. S., Shprits, Y. Y., & Spasojević, M. (2017). Empirical modeling of the plasmasphere dynamics using neural networks. *Journal of Geophysical Research: Space Physics*, *122*(11), 11227–11244. https://doi.org/10.1002/2017JA024406

Zong, Q.-G., Wang, Y. F., Zhang, H., Fu, S. Y., Zhang, H., Wang, C. R., et al. (2012). Fast acceleration of inner magnetospheric hydrogen and oxygen ions by shock induced ULF waves. *Journal of Geophysical Research*, *117*(A11), A11206. https://doi.org/10.1029/2012JA018024